Active Control of Sound Transmission Through Windows With Carbon Nanotube-Based Transparent Actuators

Xun Yu, Rajesh Rajamani, *Senior Member, IEEE*, Kim A. Stelson, and Tianhong Cui, *Senior Member, IEEE*

***Abstract*—This paper explores the development of active sound transmission control systems for windows that can achieve a significant reduction in window noise transmission. Two major challenges need to be addressed in order to make the development of such noise blocking windows feasible. These are the need for a distributed actuation system that is optically transparent and the unavailability of a real-time reference signal that can be used by the active control system to provide advance information on the noise affecting the window. To address the first challenge, a transparent thin-film actuator (speaker) is first developed for the control system, which consists of a piezoelectric poly (vinylidene fluoride) (PVDF) thin film coated with compliant carbon nanotube-based transparent conductors on both sides. The developed thin-film speaker shows excellent acoustic response over a broadband frequency range, and has the advantages of being flexible, transparent, thin, and lightweight. To address the second challenge of providing a time-advanced reference signal from a moving noise source, a small microphone array distributed on the outside wall of the home is used. New noise source identification algorithms are employed, by which an appropriate microphone from the array can be chosen to provide a reference signal. Experimental results show that over 12 dB reduction in sound transmission is achieved globally in the case of broadband sound, which demonstrates the effectiveness of the control system in blocking sound transmission.**

***Index Terms*—Active noise control (ANC), carbon nanotubes, noise source identification, sound transmission, transparent thin-film actuator, windows.**

I. Introduction

THE continued growth in urban population has led to high-density housing close to airports and highways. This has increased the exposure of the population to noise from a variety of sources, increasing the need to provide better sound insulation for the homes. For homes close to airports and highways, windows constitute the primary path through which noise enters a home. Therefore, window improvements provide the most satisfaction to home dwellers [1]. This paper explores the development of double-glazed windows with embedded active control systems to achieve significant reduction in noise transmission, especially for low frequency airport noise.

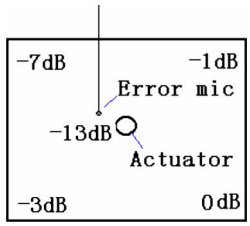

Fig. 1. ANC performance at different locations behind a 175×175 mm^2 glass panel using a point force actuator (primary noise is 600 Hz).

One major challenge for an active noise control (ANC) system for windows is the special requirement on the actuation system, which needs to be transparent. Several researches have tried innovative approaches to avoid the requirement on transparency. One approach that has been investigated by other researchers is to place loudspeakers on the sides of the cavity of double-glazed windows as secondary sources [2]–[4]. However, this cavity control approach is not effective in controlling panel radiation-dominated sound [5]. The other approach is to use a small voice-coil actuator to vibrate the glass panel itself to generate the canceling sound [6]. Although significant reduction in noise transmission is possible at the location of actuator, global noise cancellation over the entire panel cannot be achieved for high frequency noise. For instance, as shown in Fig. 1, the reduction of noise by ANC is different at different locations behind a glass panel when controlling a 600-Hz noise using a point force actuator—a reduction of 13 dB at the microphone location could be obtained but as little as 0 dB (no reduction) at some other locations. Analysis results show that uniform noise cancellation can be achieved only when the length of the panel is less than one-fifth of the wavelength of sound in the air (e.g., 0.14×0.14 m^2 for frequencies up to 500 Hz) [7]. Such a small panel is not practical for a real window application. Using multiple voice coil actuators is also not practical, since the use of several actuators on a window pane would destroy the aesthetics of the window. Hence, it is necessary to develop thin-film actuators (speakers) that can provide distributed canceling sound over the entire surface of a large sized glass panel. The need for transparency for the windows poses a great challenge to the development of such thin-film actuators.

There are no fully transparent thin-film speakers that have been previously developed, although several research groups have investigated the development of nontransparent thin-film

Manuscript received October 5, 2006. Manuscript received in final form October 25, 2006. Recommended by Associate Editor S. Devasia. This work was supported in part by Marvin Windows and Doors, Warroad, MN.

X. Yu was with the Department of Mechanical Engineering, University of Minnesota, Minneapolis, MN 55455 USA. He is now with the Department of Mechanical and Industrial Engineering, University of Minnesota, Duluth, MN 55812 USA (e-mail: xunyu@d.umn.edu).

R. Rajamani, K. A. Stelson, and T. Cui are with the Department of Mechanical Engineering, University of Minnesota, Minneapolis, MN 55455 USA (e-mail: rajamani@me.umn.edu; kstelson@me.umn.edu; tcui@me.umn.edu).

Color versions of Figs. 3–5, 7, 9, 12–14, 16–21, and 23–26 are available online at http://ieeexplore.ieee.org.

Digital Object Identifier 10.1109/TCST.2006.890277

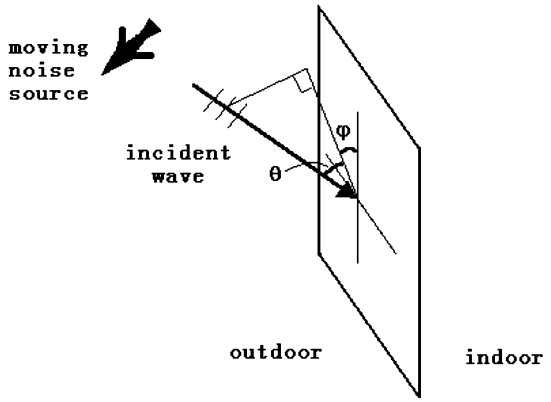

Fig. 2. Moving and oblique incident noise source (θ is the noise incident angle).

acoustic actuators. Heydt *et al.* [8], [9] developed an electroacoustic loudspeaker that uses the electrostrictive response of a polymer thin film. Over 80 dB sound pressure level can be produced from the "bubble" elements of their loudspeakers. However, the high resonant frequency (about 1500 Hz), the harmonic distortion, and the high driving electric field required (25 V/μm) will prohibit its use for most speaker applications. Piezoelectric effect is another mechanism that can be employed to fabricate loudspeakers. Among the piezoelectric polymers, PVDF has been the most studied due to its strong piezoelectric effect. Recently, PVDF has been investigated for active noise and vibration control, either being used as a sensor [10], or actuator [11], or both [12]. Results show PVDF to be a promising solution for thin-film acoustic transducers. Although PVDF itself is transparent, the need of transparency for the electrodes poses a great challenge that has not been previously solved and is addressed in this paper.

The other difficult challenge in the development of an ANC system for windows is the unavailability of a reference signal from the moving noise source for a feedforward controller. As shown in Fig. 2, a moving noise source such as an aircraft can impact the window from different directions with different incident angles. The ANC system should be able to track the moving noise source to obtain a reference signal. The reference signal must also be provided with adequate time advance to satisfy the "causality condition," i.e., the "acoustic delay" from reference microphones to panel should be bigger than the "computational and electrical delay" of the control system. We propose a microphone array that is arranged on the walls of the building at the sides of the window to obtain a reference signal from the moving noise source. Integrated with moving noise identification algorithms, as discussed in Section V, the microphone array can then track the moving noise source by detecting the noise arrival direction. An appropriate microphone can then be chosen as the reference signal for the controller.

In this paper, we develop a transparent thin-film actuator (speaker), which consists of a transparent piezoelectric PVDF thin film coated with compliant carbon nanotube-based transparent conductors on both sides. The developed thin-film actuator shows excellent acoustical response over a broadband frequency range, thus can be used for the control system. We also develop moving noise source identification algorithms

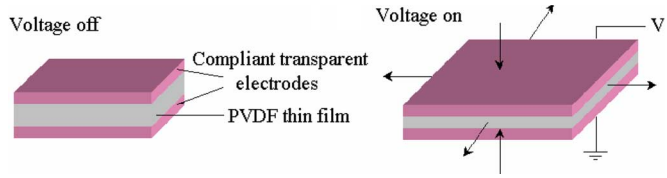

Fig. 3. Structure of the transparent thin-film actuator.

with which an appropriate microphone from a small microphone array can be chosen to provide a reference signal for the feedforward controller. The effectiveness of the control system and thin-film actuator in globally blocking sound transmission is demonstrated by experimental results.

The contents of this paper are as follows. In Section II, we discuss the development of transparent thin-film actuators. The employed FXLMS (filtered-X least mean square) control algorithm is then discussed in Section III. Next, in Section IV, we describe the experimental setup, and in Section V, we introduce two developed moving noise source identification algorithms that are used to choose an appropriate microphone for the feedforward controller. In Section VI, we present experimental results for active sound transmission control through a window. Finally, some conclusions are given in Section VII.

II. Development of Transparent Thin-Film Actuators

The proposed structure of the thin-film actuator is illustrated in Fig. 3, i.e., a piezoelectric PVDF thin film is coated with compliant transparent electrodes on both sides. When a control voltage is applied, the bending of the piezoelectric film can be used to produce the desired vibrations. As indicated before, although PVDF itself is transparent, the need of transparency and flexibility for the electrodes poses a great challenge that has not been solved and is addressed in the following.

A. Transparent Conductive Thin Films

Transparent conductive thin-film electrodes are also widely used for liquid crystal displays (LCDs), touch screens, solar cells, and flexible displays. Indium tin oxide (ITO) thin films are often used in these applications. However, ITO films needed to be deposited at high temperatures and are very brittle [13]–[15]. They are not suitable for this acoustic application since ITO films will crack and thus lose conductivity under the continuous vibration needed for an actuator. Another transparent conductive material is poly (3, 4-ethylenedioxythiophene)-poly (4-stryrenesulfonate) (PEDOT:PSS) which has good flexibility [16]. However, its low transparency and low conductivity significantly limit its performance as electrodes [17], [18]. Single-walled carbon nantotubes (SWNTs) have also been investigated for fabricating flexible transparent conductive thin films due to their high conductivity and high aspect ratio. These approaches include making SWNT/polymer composites [19], [20], wet coating surfactant-aided SWNT aqueous solutions [21], and filtering SWNT solutions [22]. However, none of these approaches satisfy the requirements for the electrodes of transparent thin-film actuators, which need to be highly conductive and highly transparent over large areas.

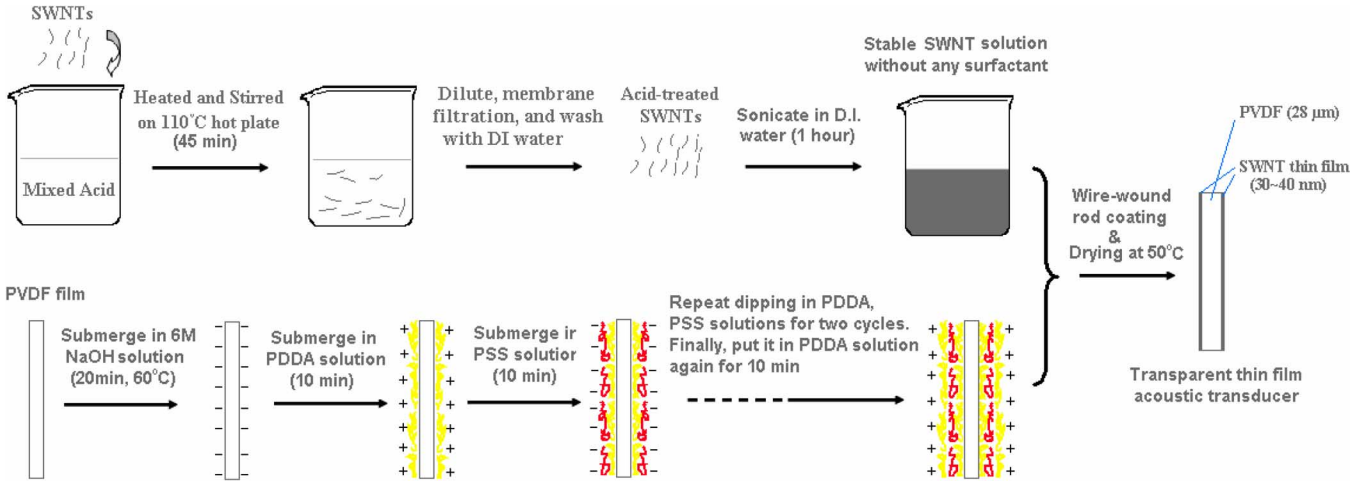

Fig. 4. Schematic diagram of the fabrication process of transparent thin-film acoustic actuator.

In this paper, we develop a unique process to fabricate transparent conductive SWNT thin films. Briefly, the process is comprised of three steps: 1) oxidizing SWNTs with a mixture of sulfuric acid and nitric acid for an adequate length of time. The negatively charged carboxylic groups introduced on the SWNT surfaces as a result of the oxidation help SWNTs to be stably dispersed in water even without any surfactant; 2) modifying the surface of the PVDF substrate using layer-by-layer (LBL) nanoassembly. Eventually, a positively charged and hydrophilic poly (diallyldimethylammonium chloride) (PDDA) molecular layer is deposited on the top of the substrate surface; and 3) coating pure SWNT thin films on to modified PVDF substrate surfaces using wet coating techniques, including wire-wound rod coating.

Both the acid treatment and LBL nanoassembly are essential to this new SWNT thin-film fabrication process. The acid treatment removes the surfactant in the films which greatly enhances the conductivity while retaining excellent optical properties, while the positively charged hydrophilic surface helps to make a large size uniform SWNT thin film and increases the bonding force between SWNTs and the substrate.

B. Prototype Transparent PVDF Thin Film Speaker

The high purity SWNTs (<10% impurity) for this study were synthesized using the chemical vapor deposition (CVD) method and were supplied by Timesnanoweb (Chengdu, China). A schematic of the thin-film fabrication process is shown in Fig. 4. In a typical acid treatment procedure, 100-mg nanotubes were added to 40 mL of acid mixture of sulfuric acid (98 wt%) and nitric acid (69 wt%) in a ratio of 3:1, and stirred for 45 min on a 110°C hot plate. The suspension was then diluted to 200 mL. Finally, the SWNTs were collected by membrane filtration (0.45 μm pore size), and washed with enough deionized (DI) water to remove residual acids. The acid treated SWNTs (10 mg) were added into 10 mL of DI water and bath ultrasonicated for 1 h and settled for a few hours at room temperature.

The substrate, 250 mm×190 mm × 28 μm PVDF thin film (Measurement Specialties Inc, VA), was first hydrolyzed with 6-M NaOH aqueous solution for 20 min at 60 °C. After rinsing with DI water, the PVDF film was immersed in 1.5 wt% PDDA solution (with 0.5-M NaCl) for 15 min at room temperature, followed by rinsing with DI water. PVDF film was then dipped into 0.3 wt% poly (sodium styrenesulfonate) (PSS) (with 0.5-M NaCl) for 15 min and rinsed. The PDDA/PSS adsorption treatment was repeated for two cycles and finally treated with PDDA solution again. The outer most layer is, thus, the positively charged PDDA molecular layer. The SWNT/water solutions was then applied to both sides of the PVDF film by wire-wound rod coating and dried at 50 °C. After drying, additional SWNT layers could be coated above the initial SWNT layer to achieve a desired combination of electrical and optical properties. The final SWNT thin film is about 30∼40 nm thick, with a surface resistivity of 2.5 kΩ/□.

Fig. 5. Photograph of the fabricated film speaker.

Fig. 5 shows a picture of a fabricated thin-film speaker fixed in a photo frame (the gray lines on the edges of the film are 3-M 9713 conductive tape which is used to reduce the electrode contact resistance). It is obvious that we can clearly see through this flexible thin-film actuator. Fig. 6 is a scanning electron microscope (SEM) image of the SWNT film, which shows a randomly ordered tight network of carbon nanotubes formed on the surface. Since there is no surfactant in the SWNT thin film, the

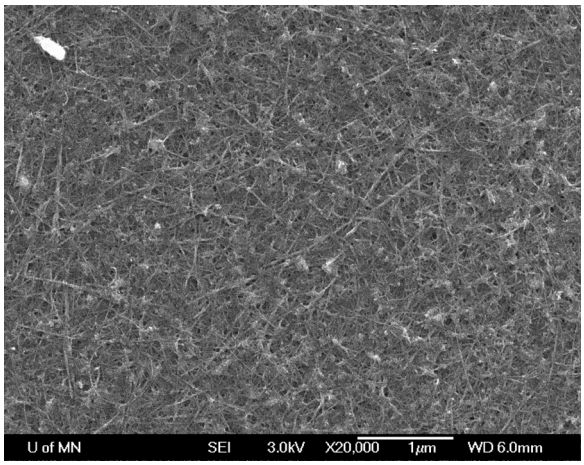

Fig. 6. SEM image of the SWNT network of the SWNT conductive thin film.

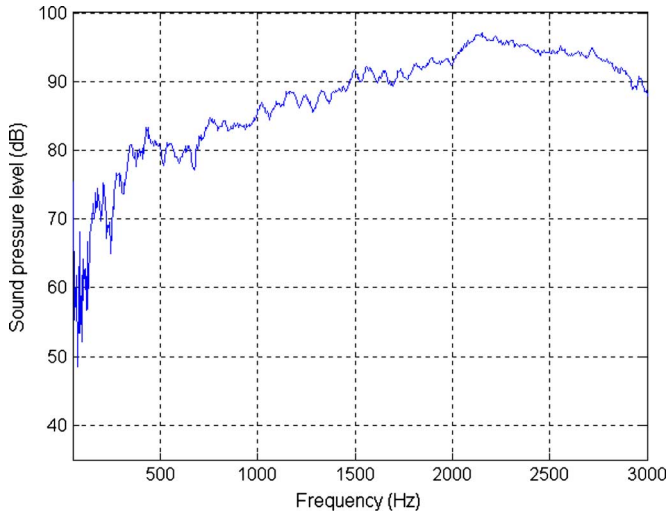

Fig. 7. Measured frequency response from the thin-film speaker that is excited by a 12-Vrms white noise signal.

SWNT bundles contact each other directly which greatly enhances the conductivity.

Fig. 7 shows a typical frequency response from 50 Hz to 3 kHz generated from the curved thin-film speaker excited by a 12 Vrms white noise signal. The response is measured at 50 mm from the speaker along the centerline axis. As can been seen from Fig. 7, the resonant frequency is about 150 Hz, which is much lower than other reported thin-film speakers in [8], [9], [17], and [18], and it is low enough for many ANC applications and general-purpose loudspeakers. Compared to other reported thin-film speakers, this speaker also requires a much lower drive voltage (about 1/8∼1/50), which removes the need for expensive high-power voltage amplifiers and results in much less power consumption.

III. Control Algorithm

The feedforward filtered-X least mean square (FXLMS) algorithm is utilized for active noise cancellation in this paper. More

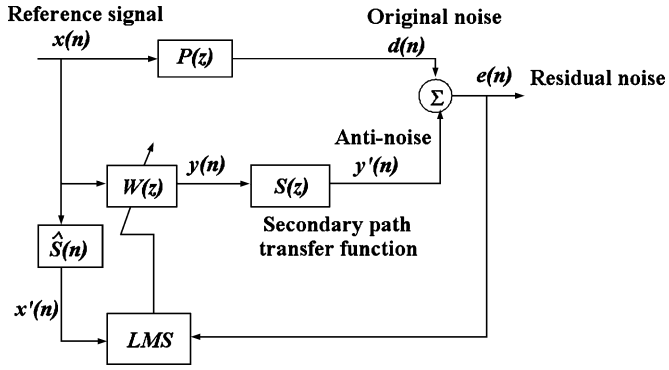

Fig. 8. Block diagram of the FXLMS feedforward control [23].

detailed discussion of the algorithm can be found in [23]. The block diagram of the FXLMS algorithm is illustrated in Fig. 8.

Here, $x(n)$ is the reference signal, $y(n)$ is the desired control (speaker) signal, $y'(n)$ is the actual sound of the secondary source, $d(n)$ is the undesired primary noise, $e(n)$ is the residual noise at downstream measured by an error microphone, $x'(n)$ is the filtered version of $x(n)$, $P(z)$ is the unknown transfer function between the reference microphone and the secondary source, $S(z)$ is the dynamics from the secondary source to the error microphone, $\hat{S}(z)$ is the estimation of this secondary path, which is offline identified following the method described in [23], and $W(z)$ is the digital filter that is adapted to generate the correct control signals to the secondary source. The objective is to minimize $e(n)$ via minimizing the instantaneous squared error $\hat{\xi}(n) = e^2(n)$. The most widely used method to achieve this is the FXLMS algorithm, which updates the coefficients of $W(z)$ in the negative gradient direction with appropriate step size μ (μ is set to be 1×10^{-10} in our program)

$$w(n+1) = w(n) - \frac{\mu}{2}\nabla\hat{\xi}(n) \tag{1}$$

where $\nabla\hat{\xi}(n)$ is the instantaneous estimate of the mean square error gradient at time n, and can be expressed as

$$\begin{aligned}\nabla\hat{\xi}(n) &= 2\left[\nabla e(n)\right]e(n) = 2\left[-s(n) * x(n)\right]e(n)\\ &= -2x'(n)e(n).\end{aligned} \tag{2}$$

By substituting the previous equation back into (1), we have the fixed-X least mean square algorithm

$$w(n+1) = w(n) + \mu x'(n)e(n) \tag{3}$$

where $x'(n)$ is estimated as $\hat{s}(n) \times x(n)$.

Once the filter coefficients $\overline{w}(n)$ have been updated, the active noise canceling control signal $y(n)$ is then obtained as

$$y(n) = W(z)x(z) = \sum_{l=0}^{L-1} w_l(n)x(n-l) \tag{4}$$

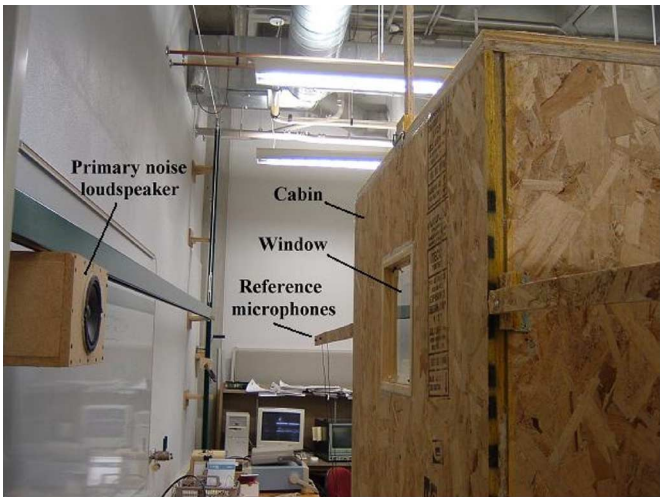

Fig. 9. Experimental setup.

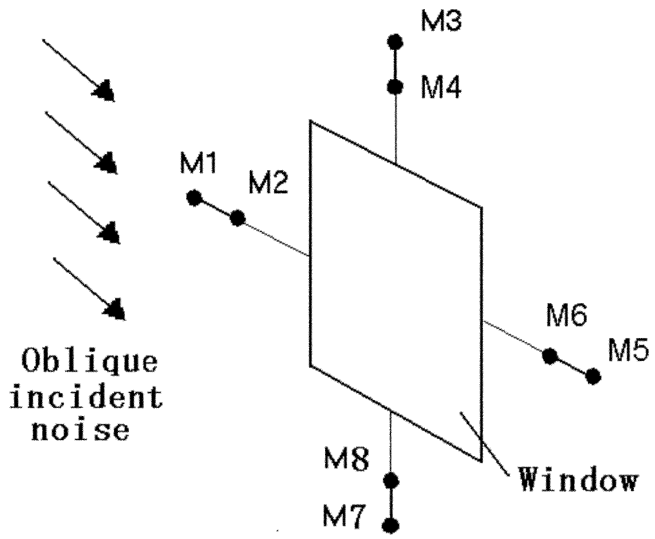

Fig. 10. Microphone array for acquiring a reference signal using TDOA method.

where L is the length of the filter, which is set to be 48 in our programs.

The control signal $y(n)$ is then sent to the actuator, which produces the antinoise sound $y'(n)$.

IV. Experimental Setup

A photograph of the experimental setup for sound transmission control is shown in Fig. 9. In the experiments, a woofer speaker that is controlled to move along a track was used to generate the primary noise and simulate the moving noise source. The vertical position of the track can also be adjusted, so as to give desired loudspeaker height. A $1.1\times 0.9\ \times\ 2\ \mathrm{m}^3$ cabin with a $200\times 200\ \mathrm{mm}^2$ window in one side built to simulate a room under the impact of noise. The reference microphone array was arranged on the sides of the window (the detailed microphone array pattern and associated noise source identification algorithm will be discussed in the Section V). The thin-film speaker was located behind the windowpane and was controlled to cancel the primary noise. A microphone behind the window panel is used to measure the residual sound pressure which is then controlled to zero (the thin-film speaker and the error microphone are behind the windowpane, thus, not shown in the photograph). An analog circuit provides functions of amplification and filtering. A CIO-DAS6402/12 data acquisition is used for data communication between a PC and speakers/microphones. The control algorithm is implemented via a PC real-time toolbox with Turbo C used to develop the real-time code. The sampling period is 150 μs.

V. Reference Signal From a Moving Noise Source for Feedforward Control

For the feedforward FXLMS control discussed in Section III, a reference signal $x(n)$ with adequate time advance is needed, so as to satisfy the "causality condition," i.e., the "acoustic delay" from reference microphones to panel should be bigger than the "computational and electrical delay" of the control system. Especially, since the aircraft noise is moving all the time and can impact windows from different directions with different incident angles, the ANC system should also be able to track the moving noise source to obtain a reference signal.

We propose a microphone array that is flush mounted on the outside walls of the building at the sides of the window to obtain the reference signal. The microphone array pattern is shown in Figs. 10 and 14 for two different noise source identification algorithms that have been developed. Because the microphones do not protrude from the outside wall, the microphones will not disturb the aesthetics of the window or the building. Most importantly, the microphones will only detect the incident acoustic pressure without any "pollution" from the acoustical wave reflected by walls and the acoustical wave produced by the actuator itself. The microphones can also provide a reference signal with adequate time advance, except at the case of normal incidence ($\theta = 90°$). Since aircraft will fly higher than the windows, it is unlikely that the noise will hit the windows with $\theta = 90°$, thus the ineffectiveness for normal incidence will not be a practical problem.

A. Detection of Noise Arrival Direction Using a Time-Difference of Arrival (TDOA)-Based Algorithm

To detect the noise arrival direction and determine which microphone from the array is to be used for obtaining the reference signal, two signal processing algorithms and associated microphone array patterns are proposed. The first one is the TDOA-based algorithm (the associated microphone array pattern is shown in Fig. 10), which evaluates the delay of the received signal in a microphone pair. As illustrated in Fig. 11, a time delay between the acoustic signal $M3$ and $M4$ of Fig. 10 will correspond to a specific ΔL related to the incident angle by $\theta = \cos^{-1}(\Delta L/h)$, where h is known. Note that two microphones have to be used in each side of the window and the distance h between them should be smaller than half of the acoustical wavelength in the interested frequency range, so that the delayed wave will not be interpreted as an advanced wave by the algorithm (for example, in Fig. 12, the first wave of $M4$ is

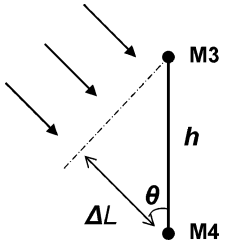

Fig. 11. TDOA-based method for estimation of noise incident angle.

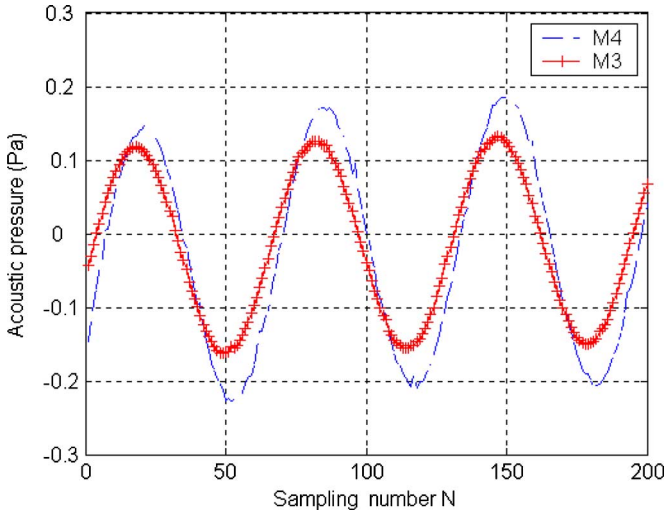

Fig. 12. Acoustic signals received by $M3$ and $M4$ of Fig. 11.

the delayed wave of the first wave of $M3$, instead of being the advanced wave of the second wave of $M3$).

To find the TDOA of a microphone pair, the cross-correlation series is calculated for the received signals by the microphone pair. The time delay is then calculated as the position where maximum cross-correlation locates. For instance, the acoustic signals received by $M3$ and $M4$ of Fig. 11 is shown in Fig. 12. The unbiased raw cross-correlation is then calculated as

$$\hat{R}_{xy}(m) = \begin{cases} \frac{1}{N-|m|} \sum_{n=0}^{N-m-1} x_{n+m} y^*, & m \geq 0 \\ \hat{R}^*_{yx}(-m), & m < 0 \end{cases} \quad m = 0, 1, 2, 3, \ldots \tag{5}$$

where x is the acoustical pressure of $M3$ and y is the acoustical pressure of $M4$.

The results are plotted in Fig. 13 for the previous single acoustic frequency test. In this test, the maximum cross-correlation value corresponds to a cross-correlation index of three as seen in Fig. 13. This index number times the sampling period will give the TDOA. Once TDOA is known, the incident angle can then be found.

The previous description of the TDOA method is using a single sine wave signal as an example for the purpose of better description. This TDOA method is also applicable to random noise. Fig. 14 shows an example of random noise received by $M3$ and $M4$, and the corresponding cross-correlation series results. It is clear that the time delay between $M3$ and $M4$ can be accurately measured.

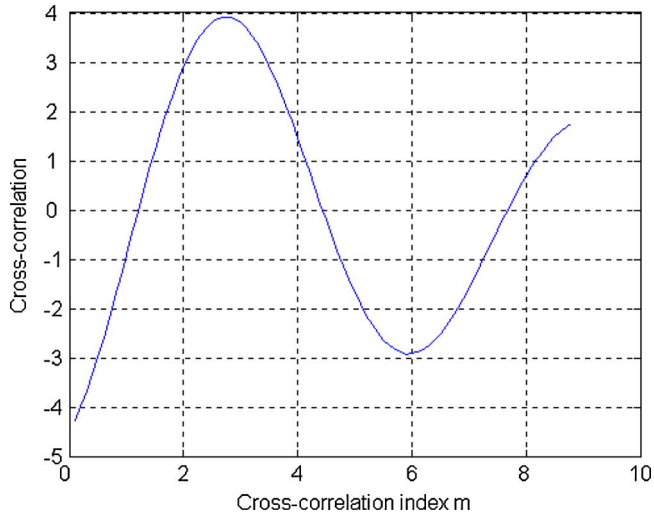

Fig. 13. Cross-correlation series of the two signals in Fig. 11.

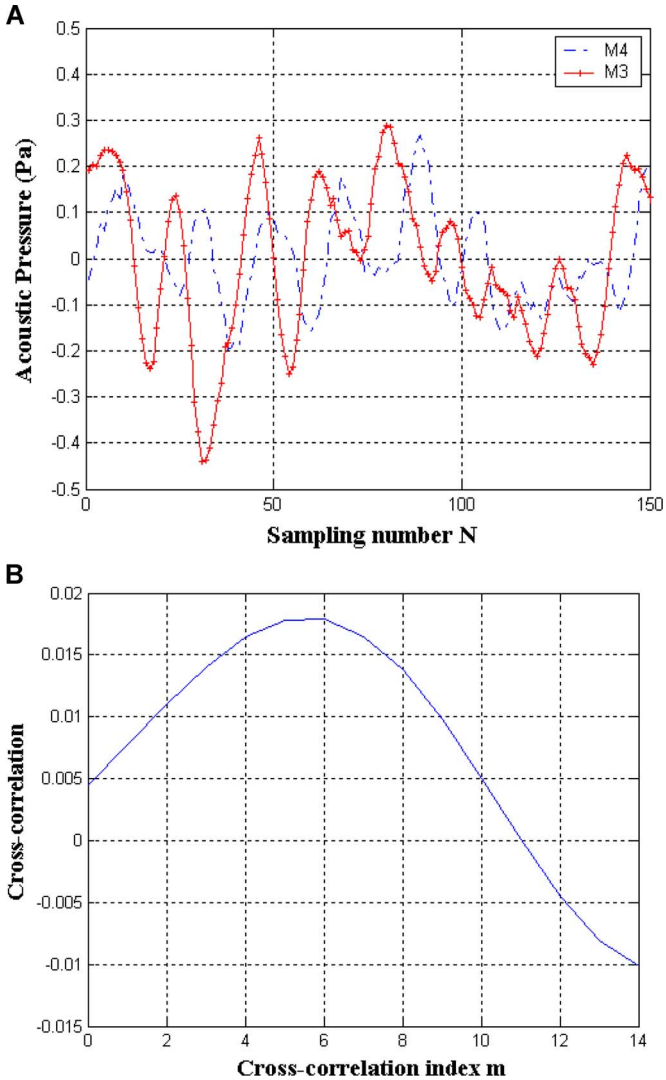

Fig. 14. (a) Random acoustic signal received by $M3$ and $M4$ and (b) the corresponding cross-correlation series.

This TDOA-based method has been experimentally tested to measure incident angles under the random noise environments.

TABLE I
EXPERIMENTAL RESULTS OF MEASURING INCIDENT ANGLES USING THE TDOA-BASED METHOD

Real incident angle (°)	Angles calculated by TDOA-base method (°)
23.95	30.3
31.9	36.4
41	46.5
54.3	56

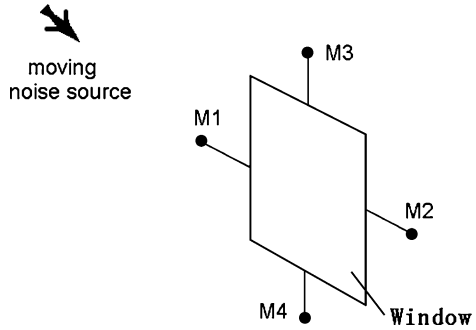

Fig. 15. Microphone array for acquiring the reference signal.

Table I lists some results, which show that the TDOA-based method can give good approximations for the incident angles. One major reason for the measurement error is due to the relatively long sampling period. A sampling period of 100 μs is used here, which corresponds to 34 mm in ΔL for every sampling period delay. Better measurement resolution will be obtained if a higher sampling rate were to be used. Here, for the purpose of the ANC algorithm, a rough estimate of the incident angle is adequate to indicate which microphone to use as the reference signal.

B. Choice of an Appropriate Reference Microphone for Feedforward Control

Using the previous TDOA-based method, the control system can effectively choose an appropriate microphone to use as the reference signal. However, the calculation of the cross-correlation induces a heavy computational load on the real-time program, which leads to slow real-time control. A more efficient computational method is desired for better active noise cancellation performance.

It is clear that the best reference signal for the feedforward controller will be the microphone that has the most time-advanced information of the noise affecting the window. In other words, if the control system can determine the microphone that is closest to the noise source, this microphone can then be used as the reference signal. Note that the sound intensity decreases as the square of the distance from the noise source [24]. Hence, the further the microphone from the noise source, the smaller acoustical pressure the microphone receives. Based on this fact, the microphone with the highest root-mean-square acoustical pressure value will be the microphone that is the closest to the noise source and will be the best reference signal for the feedforward controller.

The associated microphone array pattern for this method is shown in Fig. 15. Compared to the microphone array for TDOA method, only four microphones are needed for this method.

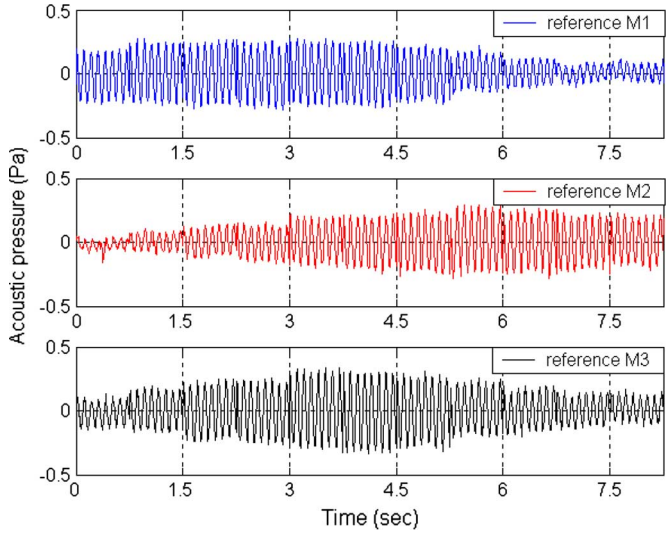

Fig. 16. Acoustic pressures measured by microphone $M1$, $M2$, and $M3$ when a noise source travels from the left-side of the window to the right-side of the window.

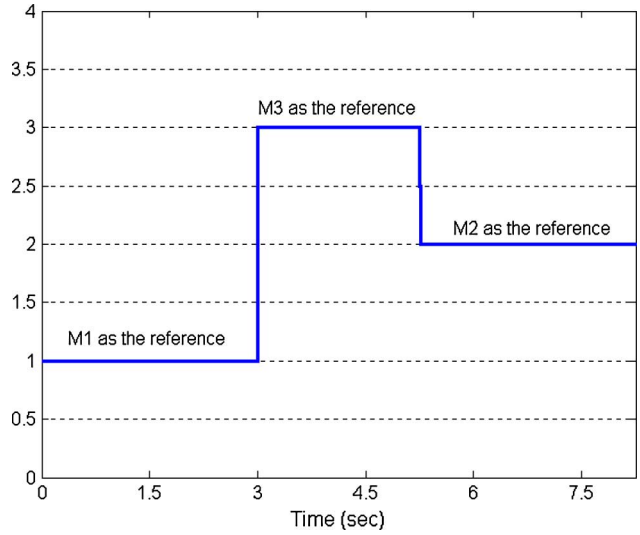

Fig. 17. Switching of the reference microphone when a noise source travels from the left-side the window to the right-side of the window.

The root-mean-square value of the acoustical pressure received by a microphone at time i is calculated as

$$P_{\text{rms}}(i) = \sqrt{\frac{\sum_{n=0}^{N} [P(i-n)]^2}{N}} \tag{6}$$

where P is the acoustical pressure and N is the computational window size, i.e., the acoustical pressure in previous N cycles are used for the calculation. A small window size N can not eliminate impulse signal noise, while a large N can not adequately reveal the real-time information. Here, the N is set to 80 for a balanced performance. To eliminate the impact of impulse signal noise, the measured acoustical pressures are also high-pass filtered before being used for calculation. The program calculates in real time and compares the root-mean-square values

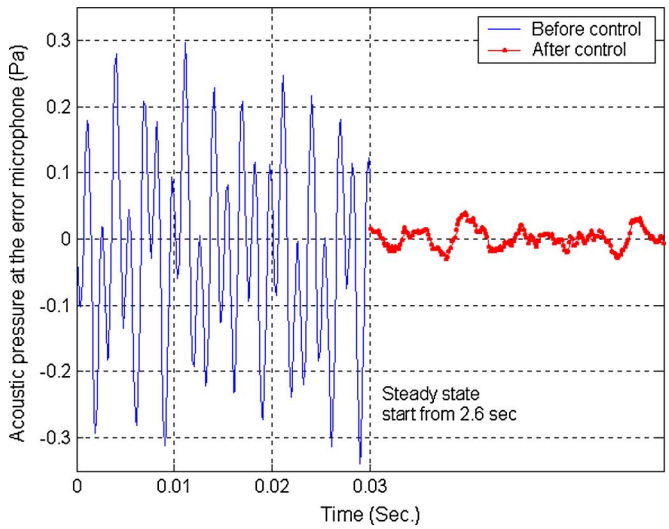

Fig. 18. Experiment results of sound transmission control (primary noise consists of frequency components 300 and 700 Hz).

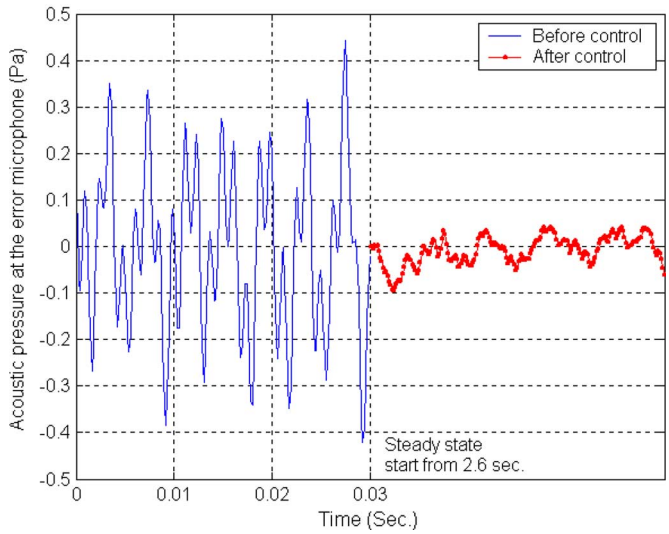

Fig. 19. Experiment results of sound transmission control (primary noise consists of frequency components 250, 450, and 800 Hz).

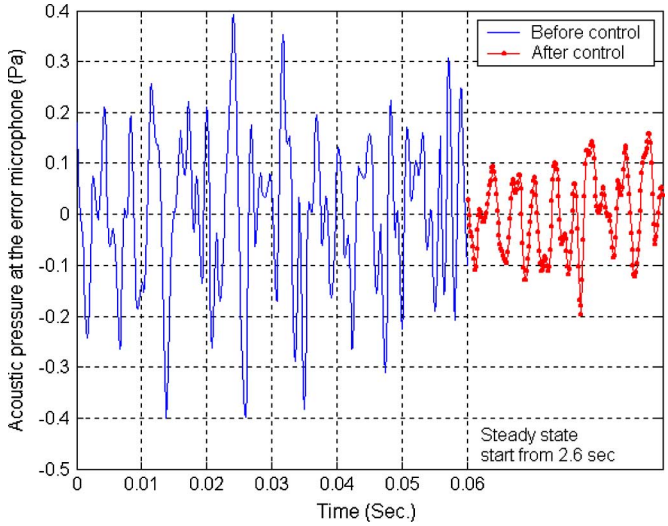

Fig. 20. Experiment results of sound transmission control—shown in time domain (the primary noise is a 0∼800-Hz random noise).

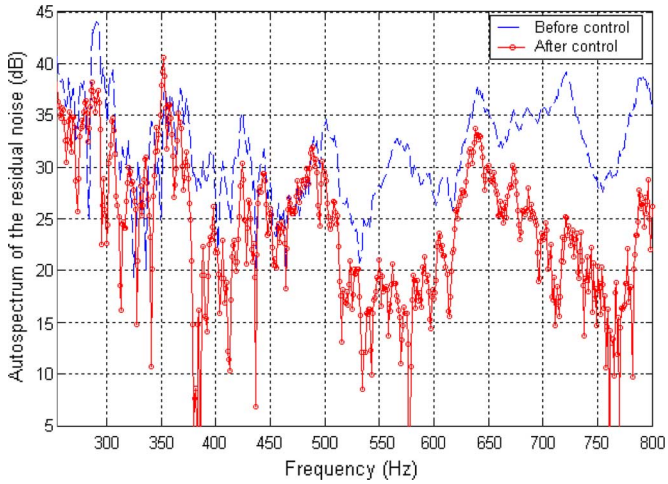

Fig. 21. Experiment results of sound transmission control—shown in frequency domain.

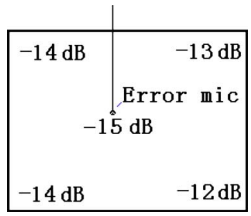

Fig. 22. Uniform ANC performance achieved at different locations behind a 200×200 mm^2 glass panel by using the transparent thin-film speaker (primary noise is 600 Hz).

of microphones, then determines an appropriate microphone (the microphone with the highest root-mean-square value) for the feedworward contoller.

This reference microphone choice algorithm is experimentally evaluated. Fig. 16 shows an example of the acoustic pressures received by microphone $M1$, $M2$, and $M3$ when a moving noise source traveled from the left-side of the window to the right-side of the window (in this example, the noise source is above the window, the information of $M4$ is not necessary and is omitted here). Fig. 17 shows the microphones chosen by the program for the controller during the noise source movement (value$=1$ stands for $M1$ as the reference, value$=2$ means $M2$ as the reference, and value$=3$ means $M3$ as the reference). As can been seen, the program can effectively choose the appropriate reference for the feedforward controller, i.e., using $M1$ when the noise source is in the left-side of the window, switching to $M3$ when the noise source moves closer to the window, and switching to $M2$ when the noise source moves away from the window to the right-side of the window. As expected, the feedforward controller gets the most time-advanced reference information all the time.

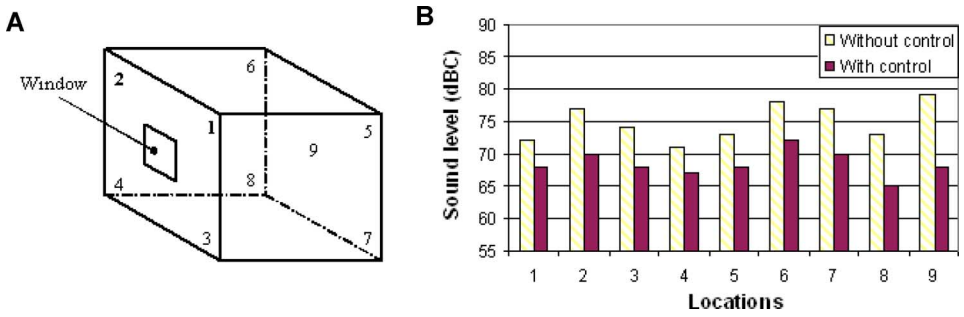

Fig. 23. (a) Schematic of the sound level measurement locations inside the room. (b) Sound levels in different locations without/with control.

VI. Experimental Results

A. Performance of the Transparent Thin Film Actuator for Active Sound Transmission Control

The experimental performance of the transparent thin-film actuator is first tested in the case of a noise source that is not moving. Figs. 18 and 19 show the performance of the transmission control system when the primary noise consists of multifrequency components. As can be seen in the figures, the residual acoustic pressure at the error microphone is significantly reduced by a factor of more than six in all cases. The measure sound reductions are about 15 dB. In Figs. 20 and 21, the primary noise consists of random noise band-limited to frequencies below 800 Hz. Fig. 20 shows the transmitted sound before and after control in the time domain. As can be seen, the control system is able to attenuate the random primary noise by more than a factor of two. The performance for controlling the random noise is also illustrated through frequency response plots in Fig. 21. The primary noise is reduced at almost every frequency. Although there is less reduction for the frequencies below 500 Hz, the thin-film speaker shows a great performance above 500 Hz. The reason of less sound reduction in low frequencies is due to the weaker acoustic response of the thin-film speaker in the low frequency range.

Most importantly, uniform noise cancellation can be achieved by using the transparent thin-film speaker. Compared to the results achieved by a point force actuator (Fig. 1), Fig. 22 shows that similar noise reduction level is achieved everywhere behind the windowpane by using the thin-film speaker. Fig. 23 shows the sound levels inside the room in nine different locations without/with control. It can be seen that the noise is reduced everywhere inside the room. Therefore, global noise level reduction, which is impossible to achieve with a point force actuator, is achieved by using the developed transparent thin-film actuators.

B. Experimental Results of Control With a Moving Noise Source

The performance of the combination of the transparent thin-film actuator and the noise source identification algorithms are tested by control in the case of a moving noise source. In a typical test, like the example in Section V-B, the primary noise moves from one side of the window to the other side of the window, and the sound level behind the windowpane is recorded. Because our program cannot take down all the data for the test (6666 data points for every second, and running time is 10 s), we take down the acoustic pressure for 100 points at the beginning of every second instead. The test was run for both situations of without and with control system being on.

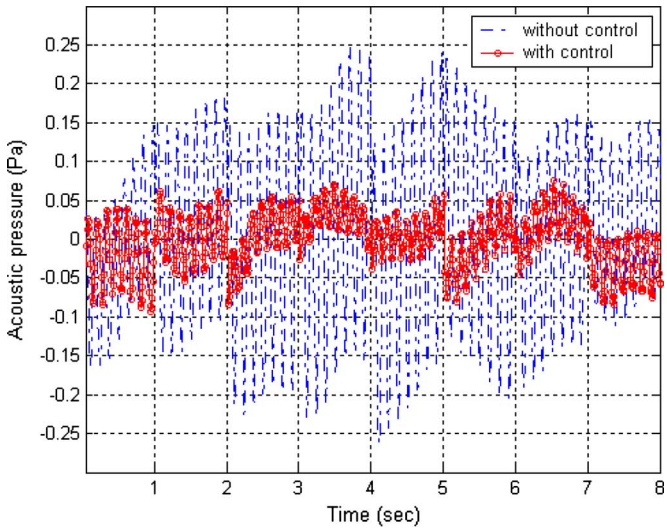

Fig. 24. Acoustical pressure behind the windowpane with and without ANC under the impact of a 500-Hz moving noise.

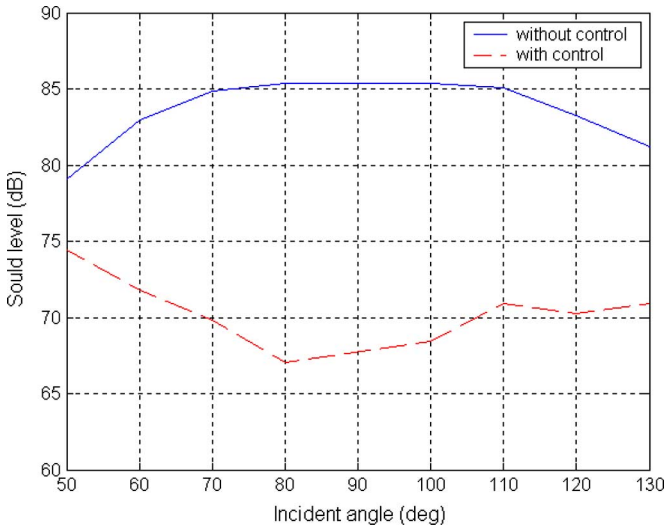

Fig. 25. Sound level behind the windowpane with and without ANC for a moving noise with different incident angles.

Fig. 24 shows the acoustical pressure behind the windowpane without and with control for a 500 Hz sound that travels from one side of the window to the other side (the switching

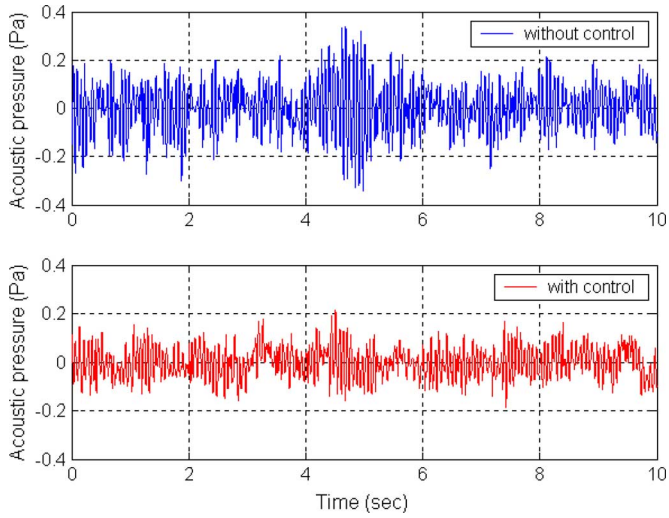

Fig. 26. Acoustical pressure behind the windowpane with and without ANC under the impact of a random moving noise (0∼800 Hz).

of reference microphones during the noise source movements is demonstrated in Section V-B). Fig. 25 shows the results in sound levels (dB) at different incident angles (different instants time in Fig. 24 corresponds to different incident angles in Fig. 25). From the results, it is clear that the ANC system is effective for controlling the moving noise from different incident angles. Note that for the noise with small incident angles ($< 50°$ and $> 130°$), because there is much less sound pressure impact on the window, the ANC system is not necessary.

The ANC system is also used to control a moving noise that consists of random noise up to 800 Hz (Fig. 26). As can be seen, the control system can attenuate the random noise by a factor of about two, which corresponds to a performance of about 6 dB in sound level reduction.

VII. Conclusion

An active sound transmission control system for windows has been successfully developed by developing transparent thin-film acoustic actuators and using a microphone array for moving noise source identification. The carbon nanotube-based transparent conductive thin films significantly enhanced the acoustic response of the thin-film transducers. With the advantages of being flexible, transparent, and lightweight, the thin-film speakers show to be a promising solution for sound transmission control for windows. The employed microphone array provides a time-advanced reference signal for the controller, thus enabling the ANC system to control a moving primary noise. It was experimentally demonstrated that global sound reduction can be achieved with the transparent thin-film speaker by using moving noise source identification.

References

[1] W. A. Utley, I. B. Buller, E. C. Keighley, and J. W. Sargent, "Effectiveness and acceptability of measures for insulating dwellings against traffic noise," *J. Sound Vib.*, vol. 109, pp. 1–18, 1986.

[2] O. E. Kaiser, S. J. Pietrzko, and M. Morari, "Feedback control of sound transmission through a double glazed window," *J. Sound Vib.*, vol. 263, pp. 775–795, 2003.

[3] A. Jakob and M. Moser, "Active control of doubled-glazed windows part I: Feedforward control," *Appl. Acoust.*, vol. 64, pp. 163–182, 2003.

[4] ——, "Active control of doubled-glazed windows part II: Feedback control," *Appl. Acoust.*, vol. 64, pp. 183–196, 2003.

[5] S. M. Kim and M. J. Brennan, "Active control of harmonic sound transmission into an acoustic enclosure using both structural and acoustic actuators," *J. Acoust. Soc. Amer.*, vol. 107, pp. 2523–2534, 2000.

[6] H. Zhu, R. Rajamani, and K. A. Stelson, "Active control of acoustic reflection, absorption and transmission using thin panels," *J. Acoust. Soc. Amer.*, vol. 113, pp. 852–870, 2003.

[7] X. Yu, H. Zhu, R. Rajamani, and K. A. Stelson, "Acoustic transmission control using active panels: An experimental study of its limitations and possibilities," presented at the Int. Symp. Flexible Autom., Osaka, Japan, 2006.

[8] R. Heydt, R. Kornbluh, R. Pelrine, and V. Mason, "Design and performance of an electrostrictive-polymer-film acoustic actuator," *J. Sound Vib.*, vol. 215, pp. 297–311, 1998.

[9] R. Heydt, R. Pelrine, J. Joseph, J. Eckerle, and R. Kornbluh, "Acoustical performance of an electrostrictive polymer film loudspeaker," *J. Acoust. Soc. Amer.*, vol. 107, pp. 833–839, 2000.

[10] R. L. Clark, R. A. Burdisso, and C. R. Fuller, "Design approaches for shaping polyvinylidene fluoride sensors in active structural acoustic control (ASAC)," *J. Intell. Mater. Syst. Structures*, vol. 4, pp. 354–365, 1993.

[11] C. Guigou and C. R. Fuller, "Adaptive feedforward and feedback methods for active/passive sound radiation control using smart foam," *J. Acoust. Soc. Amer.*, vol. 104, pp. 226–231, 1998.

[12] P. Gardonio, Y. S. Lee, and S. J. Elliott, "Analysis and measurement of a matched volume velocity sensor and uniform force actuator for the active structural acoustic control," *J. Acoust. Soc. Amer.*, vol. 110, pp. 3025–3031, 2001.

[13] Y. Hu, X. Diao, C. Wang, W. Hao, and T. Wang, "Effects of heat treatment on properties of ITO films prepared by RF magnetron sputtering," *Vacuum*, vol. 75, pp. 183–188, 2004.

[14] X. W. Sun, H. C. Huang, and H. S. Kwok, "On the initial growth of indium tin oxide on glass," *Appl. Phys. Lett.*, vol. 68, pp. 2663–2665, 1996.

[15] D. R. Cairns, R. P. Witte, II, D. K. Sparacin, S. M. Sachasman, D. C. Paine, G. P. Crawford, and R. R. Newton, "Strain-dependent electrical resistance of tin-doped indium oxide on polymer substrates," *Appl. Phys. Lett.*, vol. 76, pp. 1425–1427, 2000.

[16] D. R. Cairns, S. P. Gorkhali, S. Esmailzadeh, J. Vedrine, and G. P. Crawford, "Conformable displays based on polymer-dispersed liquid-crystal materials on flexible substrates," *J. Soc. Inf. Display*, vol. 11, pp. 289–295, 2003.

[17] C. S. Lee, J. M. Kim, D. E. Lee, J. Joo, B. G. Wagh, S. Han, Y. W. Beag, and S. K. Koh, "Flexible and transparent organic film speaker by using highly conducting PEDOT/PSS as electrode," *Synthetic Metals*, vol. 139, pp. 457–461, 2003.

[18] C. S. Lee, J. M. Kim, D. E. Lee, J. Joo, S. Han, B. G. Wagh, and S. K. Koh, "An approach to durable poly (vinylidene fluoride) thin film loudspeaker," *J. Mater. Res.*, vol. 18, pp. 2904–2911, 2003.

[19] P. J. Glatkowski, "Carbon nanotube based transparent conductive coating," in *Proc. 48th Int. SAMPE Symp.*, 2003, pp. 2146–2152.

[20] J. G. Smith, Jr., J. W. Connell, D. M. Delozier, P. T. Lillehei, K. A. Watson, W. Lin, B. Zhou, and Y.-P. Sun, "Space durable polymer/carbon nanotube films for electrostatic charge mitigation," *Polymer*, vol. 45, pp. 825–836, 2004.

[21] N. Saran, K. Parikh, D.-S. Suh, E. Munoz, H. Kolla, and S. K. Manohar, "Fabrication and characterization of thin films of single-walled carbon nanotube bundles on flexible plastic substrates," *J. Amer. Chem. Soc.*, vol. 126, pp. 4462–4463, 2004.

[22] Z. Wu, Z. Chen, X. Du, J. M. Logan, J. Sippel, M. Nikolou, K. Kamaras, J. R. Reynolds, D. B. Tanner, A. F. Hebard, and A. G. Rinzler, "Transparent, conductive carbon nanotube films," *Science*, vol. 305, pp. 1273–1276, 2004.

[23] S. M. Kuo and D. R. Morgan, *Active Noise Control Systems—Algorithms and DSP Implementations*. New York: Wiley, 1996.

[24] L. L. Beranek, Ed., *Noise and Vibration Control*. Washington, DC: Inst. Noise Control Eng., 1988, pp. 14–16.

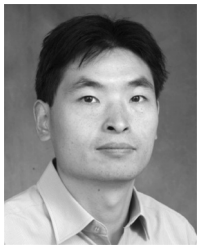

Xun Yu received the Ph.D. degree in mechanical engineering from the University of Minnesota, Minneapolis, in 2006.

After graduation, he joined the Department of Mechanical and Industrial Engineering, University of Minnesota, Duluth, as an Assistant Professor. His research interests include active noise control, mico/nano systems, and carbon nanotube-based sensors and actuators.

Rajesh Rajamani (SM'06) received the B.Tech. degree from the Indian Institute of Technology, Madras, India, in 1989 and the M.S. and Ph.D. degrees from the University of California at Berkeley, in 1991 and 1993, respectively.

He is currently an Associate Professor in the Department of Mechanical Engineering at the University of Minnesota, Minneapolis. After receiving the Ph.D. degree, he worked as a Research Engineer, first at United Technologies Research Center (UTRC) and then at California PATH, University of California at Berkeley. His research interests include sensor development and control system design for automotive and biomedical applications. He has authored over 85 refereed publications and received four patents.

Dr. Rajamani is a recipient of several awards including the CAREER Award from the National Science Foundation, the 2001 Outstanding Paper Award from the IEEE TRANSACTIONS ON CONTROL SYSTEMS TECHNOLOGY, the Distinguished Service Team Award from the University of California at Berkeley, and the Outstanding Achievement of the Year Award from United Technologies Research Center.

Kim A. Stelson received the B.S. degree from Stanford University, Palo Alto, CA, in 1974, and the S.M. and Sc.D. degrees from Massachusetts Institute of Technology, Cambridge, in 1977 and 1982, respectively.

He has been with the University of Minnesota, Minneapolis, since 1981. He is currently a Professor and a Director of the National Science Foundation Engineering Research Center for Compact and Efficient Fluid Power. His research interests include system dynamics, control, manufacturing, and fluid power.

Prof. Stelson is a Fellow of the American Association for the Advancement of Science.

Tianhong Cui (SM'04) received the B.S. degree from Nanjing University of Aeronautics and Astronautics, Nanjing, China, in 1991, and the Ph.D. degree from the Chinese Academy of Sciences, Beijing, China, in 1995.

He is currently an Associate Professor of Mechanical Engineering at the University of Minnesota, Minneapolis. From 1999 to 2003, he was an Assistant Professor in the Department of Electrical Engineering, Louisiana Technical University, Ruston. Prior to that, he was a STA Fellow at the National Laboratory of Metrology, and served as a Postdoctoral Research Associate at the University of Minnesota and Tsinghua University, Beijing, China. His research interests include MEMS/NEMS, nanotechnology, and polymer electronics.

Dr. Cui is a member of the American Society of Mechanical Engineers.